Journal of Statistical Physics, Vol. 124, Nos. 2-4, July/August 2006 (© 2006)
DOI: 10.1007/s10955-006-9078-y

Hydrodynamic Theory for Reverse Brazil Nut Segregation and the Non-monotonic Ascension Dynamics

Meheboob Alam,[1] L. Trujillo,[2] and H. J. Herrmann[3]

Received February 24, 2005; accepted January 31, 2006
Published Online: May 9, 2006

Based on the Boltzmann–Enskog kinetic theory, we develop a hydrodynamic theory for the well known (reverse) Brazil nut segregation in a vibrofluidized granular mixture. Under strong shaking conditions, the granular mixture behaves in some ways like a fluid and the kinetic theory constitutive models are appropriate to close the continuum balance equations for mass, momentum and granular energy. Using this analogy with standard fluid mechanics, we have recently suggested a novel mechanism of segregation in granular mixtures based on a *competition between buoyancy and geometric forces*: the Archimedean buoyancy force, a pseudo-thermal buoyancy force due to the difference between the energies of two granular species, and two geometric forces, one compressive and the other-one tensile in nature, due to the size-difference. For a mixture of perfectly hard-particles with elastic collisions, the pseudo-thermal buoyancy force is zero but the intruder has to overcome the net compressive geometric force to rise. For this case, the geometric force competes with the standard Archimedean buoyancy force to yield a threshold density-ratio, $R_{\rho 1} = \rho_l/\rho_s < 1$, above which the *lighter intruder sinks*, thereby signalling the *onset* of the *reverse buoyancy* effect. For a mixture of dissipative particles, on the other hand, the non-zero pseudo-thermal buoyancy force gives rise to another threshold density-ratio, $R_{\rho 2}$ $(> R_{\rho 1})$, above which the intruder rises again. Focussing on the *tracer* limit of intruders in a dense binary mixture, we study the dynamics of an intruder in a vibrofluidized system, with the effect of the base-plate excitation being taken into account through a 'mean-field' assumption. We find that the rise-time of the intruder could vary *nonmonotonically* with the density-ratio. For a given size-ratio, there is a threshold density-ratio for the intruder at which it takes the maximum time to rise, and above(/below) which it rises faster, implying that *the heavier (and larger) the intruder, the faster it ascends*. The peak on the rise-time curve decreases in height and shifts to a lower density-ratio as we increase the pseudo-thermal

[1] Engineering Mechanics Unit, Jawaharlal Nehru Centre for Advanced Scientific Research, Jakkur P.O., Bangalore 560064, India; e-mail: meheboob@jncasr.ac.in
[2] Centro de Física, Instituto Venezolano de Investigaciones Centíficas, A. P. Caracas 1029-A, Venezuela.
[3] Institut für Computer Physik, Pfaffenwaldring 27, Universität Stuttgart, D-70569 Stuttgart, Germany.

buoyancy force. The rise (/sink) time *diverges* near the threshold density-ratio for reverse-segregation. Our theory offers a *unified* description for the (reverse) Brazil-nut segregation and the nonmonotonic ascension dynamics of Brazil-nuts.

KEY WORDS: Granular mixture; Brazil-nut segregation, Reverse buoyancy; Non-monotonic rise velocity.

1. INTRODUCTION

The phenomenon of segregation, in which a homogeneous mixture of particles of different species becomes spatially non-uniform by sorting themselves in terms of their size and/or mass, is ubiquitous in numerous chemical and pharmaceutical industries, dealing with the transport and handling of bulk granular mixtures.[1,2] For most industrial processes, it is required to maintain a homogeneous mixture during processing, with the segregation being the 'unwanted' phenomenon. Despite its unwanted consequences, however, segregation occurs spontaneously in driven granular mixtures.[3–13]

When a mixture of different particles is subjected to vertical shaking in a container, the larger particles (intruders) rise to the free surface. This is known as the *Brazil-nut phenomenon* (BNP), and is one of the most puzzling phenomena of granular materials research, still lacking a proper theoretical explanation. The early experimental investigations on the Brazil nut phenomenon[2,4–6] were mainly concentrated on the effect of size of the intruder particle in vibrated systems. Besides experiments, computer simulations have been extensively used to study segregation.[3,7–9] In fact, the current interest within the physics community on granular segregation was stimulated by the Monte Carlo simulations of Rosato and co-workers.[3] They explained BNP as a *percolation* effect since the smaller particles can easily percolate down to fill the void, created behind the larger particles due to external shaking, which, in turn, pushes the larger particle to the top. However, we need to point out that such percolation effects are likely to be active in a dense bed only under weak-shaking conditions.

In many experimental setups convection is unavoidable[4,6] and seems to be a key ingredient to drive segregation.[4,6,8] In the regime of convection-driven segregation,[4] it has been experimentally verified that the large particles rise with an *upward-plume* of the surrounding bed at the center of the container, but cannot sink to the bottom since they are unable to fit themselves in a narrow *downward-plume* near the side-walls. It has subsequently been verfied, via careful MD simulations,[8] that convection-driven segregation dominates (over percolation) in deep beds. In this scenario the intruder particles with different sizes rise at approximately the same rate.[4]

However, a regime where convection is negligible has also been found in some experiments[5] as well as in many idealized simulations.[3,7,9] The most

striking observation in this case is the dependence of the segregation-rate on the particle-size, where the ascending velocity of the intruder particle increases with its size.[5,7] It has been found that there is a *threshold size-ratio* for the intruder above (/below) which the intruders rise (/sink).

A series of recent discoveries have shown that the Brazil nut phenomenon is more intricate than it might seem. The subject took a major step forward with the papers of Shinbrot and Muzzio[10] and Hong *et al.*[11] In 1998 Shinbrot and Muzzio[10] discovered a *reverse buoyancy* effect: while a large heavy intruder rises to the free surface, an equally large but light intruder sinks to the bottom of the granular bed. Three years later Hong *et al.* [11] introduced a phenomenological theory for the *reverse Brazil nut phenomenon* (RBNP): a competition between percolation and condensation, depending on the size and the mobility of the intruder particles, could drive the intruders to sink to the bottom of the container and vice versa. The key idea of this theory is that a monodisperse system of particles can be fluidized above a critical temperature (T_{cr}), assuming that the system is shaken uniformly. Hence, if a binary mixture is vibrated such that the mixture temperature lies between the critical temperatures of two individual species, then one species will be in a fluidized state and the other condenses at the bottom, leading to segregation. Immediately the subject attracted the attention of researchers who performed new experiments.[12,13]

As mentioned before, different mechanisms have been proposed to explain the segregation phenomenon, for example, percolation,[3] arching,[5] convection,[4,6,8] inertia,[10] condensation[11] and interstitial-fluid effects.[12] Unfortunately, while the observational evidence accumulates,[2–10,12,13] relatively little work exists on a unified theory for the dynamics of Brazil nuts.[11,15–17] Recently, Jenkins and Yoon[17] developed a theory for the segregation of elastic particles using hydrodynamic equations of binary mixtures. They investigated the upward-to-downward transition introduced in ref. 11 even though their prediction of the phase diagram for the BNP/RBNP-transition did not match with the simulation results of Hong *et al.* Interestingly, none of these early theories considered either the non-equipartition of granular energy (which is a generic feature of granular mixtures) or the effect of external driving forces. Thus, it appears that a comprehensive theoretical description for the dynamics of Brazil nuts is still lacking.

A hydrodynamic model to include the effect of the non-equipartition of granular energy was postulated in ref. 18 where a new mechanism for segregation due to buoyant forces was introduced, drawing a direct analogy with the buoyancy forces in fluids. More recently, a *minimal* hydrodynamic model for segregation was outlined in ref. 19, starting from the Boltzmann–Enskog-level continuum equations for a dense binary mixture of fluidized granular materials. The important effect of dissipation, which is responsible for the non-equipartition of the granular energy, was also incorporated. This latter work clearly shows how one could derive a time-evolution equation for the relative rise velocity of the intruder from first principles,

thereby making the analogy with standard fluids transparent (which has a history of more than a century, with the seminal works of Stokes, Oseen, Boussinesq, etc). It was argued in ref. 19 that the BNP/RBNP segregation dynamics results from a competition between buoyancy and geometric forces. This analysis[19] appears to be compatible with the experimental observations reported by Breu *et al.*[13] and also agrees with the molecular dynamics simulations reported by Hong *et al.*[11]

In view of the good qualitative agreement of our model[19] with the experimental observations presented by Breu *et al.*,[13] it is worth attempting to construct a theory for segregation in granular materials using the kinetic theory of inelastic hard particles. We show that a *granular hydrodynamic* theory does indeed provide a good description for the dynamics of Brazil nut segregation.

This paper is organized as follows. In Section 2 we introduce the kinetic theory for inelastic hard particles, by summarizing the principal definitions of the model and presenting the balance equations for the mixture. The problem of the non-equipartition of kinetic energy is considered in 2.2.2. The main results of this paper are presented in Section 3, where the detailed theory for segregation is outlined. The evolution equation that governs the segregation dynamics of intruders in the dense collisional regime is outlined in 3.1. We then comment on the *origin* of different 'gravitational' segregation forces derived from the model in Section 3.2.1, followed by a discussion on the *origin* of the unsteady forces that act on the intruders in Section 3.2.2. In Section 4 we discuss the phase-diagram for the BNP/RBNP transition in three-dimensions (i.e. for spherical particles), thereby verifying that the competition between the buoyancy and geometric forces drives the segregation process in a fluidized mixture. In addition, we explain the *reverse buoyancy effect* of Shinbrot and Muzzio[10] in Section 4.1. In Section 5 we apply our theory to probe the dynamics of intruders in the tracer limit, thereby explaining some recent experimental observations on the *non-monotonic* rise-time[12] of the intruder (with the density-ratio) as well as the *divergence* of the rise(/sink) time near the BNP/RBNP transition. In Section 6.1 we provide a simple analytical explanation for the RBN effect, focusing on the Boltzmann (dilute) limit. In Section 6.2 we discuss the possible higher-order effects of the non-Maxwellian velocity distribution on segregation forces, along with suggestions on some experimental implications of the present work. The conclusions and the limilations of our theory are detailed in Section 7.

2. KINETIC THEORY OF GRANULAR MIXTURES

We assume that granular matter can be described at the 'macroscopic' level by a set of continuous hydrodynamic equations as a fluid–mechanical medium. The balance equations and the constitutive relations can be derived from a kinetic theory description. For granular media the kinetic equations are modified to account for the inelastic nature of the collisions between particles.[14] These equations

have been extended to binary mixtures.[20–22] The validity of the hydrodynamic approach even in the dense limit has recently been justified via a comparison of the theory with various experiments.[23]

Theoretical and numerical studies for binary granular mixtures have shown that the two components have different kinetic (fluctuation) energies[20,22,24–26] which has also been confirmed in vibrofluidized experiments.[27] Recently, Alam and Luding[24,25] have demonstrated that a proper constitutive model for granular mixtures must incorporate the effect of the non-equipartition of granular energy. Therefore, in the present model we consider this breakdown of equipartition on the kinetic energy and this is a fundamental difference with previous related studies.[11,16,17]

The following subsection intends mainly to establish some notational conventions used throughout the paper and recall some basic definitions on granular hydrodynamics. Here we follow the lines of refs. 20 and 21 in the introduction of the kinetic theory model and refs. 24 and 25 in the discussion of the breakdown of the equipartition of the kinetic energy.

2.1. Definitions

As a mechanical model for a granular fluid we consider a binary mixture of slightly inelastic, smooth particles (disks/spheres) with radii r_i ($i = l, s$, where l stands for large particles and s for small), mass m_i in two or three dimensions ($d = 2, 3$). The coefficient of restitution for collisions between particles is denoted by e_{ij}, with $e_{ij} \leq 1$ and $e_{ij} = e_{ji}$.

The average macroscopic quantities are calculated by taking appropriate moments of the corresponding microscopic (particle-level) property in terms of the single particle velocity distribution function $f_i(\mathbf{c}, \mathbf{r}, t)$ for each species. By definition $f_i(\mathbf{c}, \mathbf{r}, t)\mathrm{d}\mathbf{c}\mathrm{d}\mathbf{r}$ is the total number of particles which, at time t, have velocities in the interval d$\mathbf{c}$ centered at $\mathbf{c}$ and positions lying within a volume element d$\mathbf{r}$ centered at $\mathbf{r}$, i.e.,

$$\int f_i(\mathbf{c}, \mathbf{r}, t)\mathrm{d}\mathbf{c}\mathrm{d}\mathbf{r} = N_i.$$

If the particles are uniformly distributed in space, so that f_i is independent of $\mathbf{r}$, then the number density n_i of species i is

$$n_i = \int f_i(\mathbf{c}, \mathbf{r}, t)\mathrm{d}\mathbf{c},$$

and the total number density is $n = n_l + n_s$. The species mass density ϱ_i is defined by the product of n_i and m_i, and the total mixture density is

$$\varrho = \varrho_l + \varrho_s = \rho_l \phi_l + \rho_s \phi_s,$$

where ρ_i is the material density of species i and ϕ_i is the d-dimensional volume fraction for species i:

$$\phi_i = \frac{\Omega_d}{d} n_i r_i^d,$$

where Ω_d is the surface area of a d-dimensional unit sphere.

The mean value of any quantity $\psi_i = \psi(\mathbf{c})$ of a particle species i, is

$$\langle \psi_i(\mathbf{c}) \rangle \equiv \frac{1}{n_i} \int \psi_i(\mathbf{c}) f_i(\mathbf{c}) \mathrm{d}\mathbf{c}.$$

The mean velocity of species i is $\mathbf{u}_i = \langle \mathbf{c}_i \rangle$. The mass average velocity $\mathbf{u}$ of the mixture is defined by

$$\mathbf{u} \equiv \frac{1}{\varrho}(\varrho_l \mathbf{u}_l + \varrho_s \mathbf{u}_s).$$

The peculiar (fluctuation) velocity of species i is $\mathbf{C}_i \equiv \mathbf{c}_i - \mathbf{u}$, and the diffusion velocity is $\mathbf{v}_i \equiv \langle \mathbf{C}_i \rangle = \mathbf{u}_i - \mathbf{u}$. The species "granular temperature" is defined proportional to the mean kinetic energy of species i

$$T_i \equiv \frac{1}{d} m_i \langle \mathbf{C}_i \cdot \mathbf{C}_i \rangle,$$

and the mixture temperature is

$$T \equiv \frac{1}{n}(n_l T_l + n_s T_s).$$

Let us remark that this generalized notion of temperature is introduced for a theoretical convenience to take advantage of a thermodynamical analogy for granular materials, and thereby postulating a higher-order field variable. Even though the definition of thermodynamic variables for non–equilibrium states is straightforward theoretically, the thermodynamics of non–equilibrium states has always been a matter of debate which we will not touch upon here.

2.2. Mixture Granular Hydrodynamics

The evolution of the granular system is governed by the well known balance equations for the mixture density, momentum and energy:

$$\dot{\varrho} = -\varrho \nabla \cdot \mathbf{u}, \tag{1}$$

$$\varrho \dot{\mathbf{u}} = -\nabla \cdot \mathbf{P} + \sum_{i=l,s} n_i \mathbf{F}_i, \tag{2}$$

$$\bar{\rho} \frac{d}{2} \dot{T} = T \nabla \cdot \mathbf{j} - \nabla \cdot \mathbf{q} - \mathbf{P} : \nabla \mathbf{u} + \sum_{i=l,s} \mathbf{j}_i \cdot \mathbf{F}_i - \mathcal{D}, \tag{3}$$

where the overdot indicates the convective derivative: $\partial_t(\cdot) + \mathbf{u} \cdot \nabla(\cdot)$. Here, $\mathbf{P}$ is the mixture stress tensor, $\mathbf{F}_i$ is the external force acting on the particle, $\mathbf{q}$ is the mixture energy flux, $\mathbf{j}$ is the diffusive mass-flux and $\mathcal{D}$ is the total inelastic dissipation rate. These equations are rigorous consequences of the Enskog–Boltzmann kinetic equation,[28] extended to inelastic particles,[20,21] and must be supplemented with respective constitutive equations for $\mathbf{P}$, $\mathbf{q}$, $\mathbf{j}$ and $\mathcal{D}$. For $e_{ij} = 1$, the collisional dissipation rate vanishes ($\mathcal{D} = 0$), and consequently we recover the standard energy balance equation for a mixture of elastic hard spheres.[28].

2.2.1. Species Balance Equations and Fluxes

The species momentum balance equation is:

$$\partial_t(n_i \mathbf{u}_i) + \nabla \cdot (n_i \mathbf{u}_i \mathbf{u}_i) = -\frac{1}{m_i} \nabla \cdot \mathbf{P}_i + \frac{n_i}{m_i} \mathbf{F}_i + \Gamma_i, \tag{4}$$

where Γ_i is the momentum source which arises due to the interaction between unlike particles and $\sum_{i=l,s} \Gamma_i = \mathbf{0}$. In the limit of small spatial inhomogeneities (i.e. first order in the gradients of the mean fields) the species stress tensor $\mathbf{P}_i$ has, at the Navier-Stokes level, the standard Newtonian form

$$\mathbf{P}_i = p_i \mathbf{I} + \mu_i (\nabla \mathbf{u} + \nabla \mathbf{u}^T), \tag{5}$$

where p_i is the partial pressure of species i, μ_i is the viscosity of of species i and $\mathbf{I}$ the unit tensor. The equation of state for the partial pressure of species i can be written as:[20,21]

$$p_i = n_i Z_i T_i, \tag{6}$$

where Z_i is the "compressibility" factor of species i,

$$Z_i \equiv 1 + \sum_{j=l,s} K_{ij}, \tag{7}$$

and

$$K_{ij} \equiv \frac{1}{2} \phi_j \chi_{ij} (1 + R_{ij})^d. \tag{8}$$

Here χ_{ij} is the contact value of the radial distribution function and $R_{ij} = r_i / r_j$ the size ratio. The radial distribution functions of granular systems are often approximated by their elastic counterpart (see, for example,[20,21] and for related issues[29]). In this paper we use the following functions for disks:[30]

$$\chi_{ij} = \frac{1}{1 - \phi} + \frac{9}{8} \frac{\phi_l R_{il} + \phi_s R_{is}}{(1 + R_{ij})(1 - \phi)^2}, \tag{9}$$

and for spheres:

$$\chi_{ij} = \frac{1}{1-\phi} + \frac{\phi_l R_{il} + \phi_s R_{is}}{(1+R_{ij})(1-\phi)^2}\left[3 + \frac{2(\phi_l R_{il} + \phi_s R_{is})}{(1+R_{ij})(1-\phi)}\right]. \tag{10}$$

An explicit expression for the momentum source term can be written as:[20]

$$\Gamma_i = n_i K_{ik} T \left[\left(\frac{m_k - m_i}{m_{ik}}\right)\nabla(\ln T) + \nabla\left[\ln\left(\frac{n_i}{n_k}\right)\right] - \frac{4}{r_{ik}}\left(\frac{2m_i m_k}{\pi m_{ik} T}\right)^{1/2}(\mathbf{u}_i - \mathbf{u}_k)\right], \tag{11}$$

where $m_{ik} = m_i + m_k$ and $r_{ik} = r_i + r_k$, with $i \neq k$. In deriving the above expression, it has been assumed that the single particle velocity distribution function of species i is a Maxwellian at its own granular energy T_i:

$$f_i(\mathbf{c}, \mathbf{z}, t) = n_i\left(\frac{m_i}{2\pi T_i}\right)^{d/2}\exp\left(-\frac{m_i(\mathbf{c}-\mathbf{u}_i)^2}{2T_i}\right). \tag{12}$$

This represents the zeroth-order approximation for the distribution function which has recently been verified in molecular dynamics simulations of vibrofluidized binary granular mixtures.[31] Higher-order corrections to the distribution function would appear beyond the Euler-level description that we neglect in the present work (see discussion in VI.B).

The energy balance equation of species i is

$$\partial_t(n_i T_i) + \nabla\cdot(n_i \mathbf{u}_i T_i) + \nabla\cdot\mathbf{Q}_i + \mathbf{P}_i : \nabla\mathbf{u} - n_i\mathbf{F}_i\cdot\mathbf{v}_i - \frac{\varrho_i}{\varrho}\mathbf{v}_i\cdot(\nabla\cdot\mathbf{P}_i - n\mathbf{F}) = \mathcal{D}_i, \tag{13}$$

and the mixture energy flux is defined as

$$\mathbf{q} = \sum_{i=l,s} n_i T_i + \mathbf{Q}_i, \tag{14}$$

where $\mathbf{Q}_i$ is the energy flux of species i:

$$\mathbf{Q}_i = \kappa_i\sqrt{T_i}\nabla T_i, \tag{15}$$

and κ_i is the analog of thermal conductivity of species i. The rate of kinetic energy dissipation of species i, $\mathcal{D}_i$, is[26]

$$\mathcal{D}_i = \frac{\sqrt{2}d}{\sqrt{\pi}\Omega_d}\frac{m_i\phi_i}{r_i^{d+1}}\sum_{j=l,s}\chi_{ij}R_{ij}^d\left(1+R_{ji}\right)^{d-1}\phi_j M_{ji} \times\left[M_{ji}\left(1-e_{ij}^2\right)\left(\frac{T_i}{m_i}+\frac{T_j}{m_j}\right) + 2\left(1+e_{ij}\right)\frac{T_i - T_j}{m_{ij}}\right]\left(\frac{T_i}{m_i}+\frac{T_j}{m_j}\right)^{1/2}, \tag{16}$$

where $M_{ji} \equiv m_j/m_{ij}$. The total rate of kinetic energy dissipation is simply $\mathcal{D} = \mathcal{D}_l + \mathcal{D}_s$. We can split Eq. (16) into two terms:

1. The inter–species collisional dissipation rate, $\mathcal{D}_i^I$,

$$\mathcal{D}_i^I \equiv \frac{\sqrt{2}d}{\sqrt{\pi}\Omega_d} \sum_j \chi_{ij} R_{ij}^d (1 + R_{ji})^{d-1} M_{ji}^2 (1 - e_{ij}^2) \times \frac{\phi_i \phi_j}{r_i^{d+1}} \frac{T_i^{3/2}}{m_i^{1/2}} \left(1 + \frac{m_i T_j}{m_j T_i}\right)^{3/2}. \tag{17}$$

2. The exchange collisional dissipation rate, $\mathcal{D}_i^E$,

$$\mathcal{D}_i^E \equiv \frac{2\sqrt{2}d}{\sqrt{\pi}\Omega_d} \chi_{ik} R_{ik}^d (1 + R_{ki})^{d-1} M_{ik} M_{ki} (1 + e_{ik}) \times \frac{\phi_i \phi_k}{r_i^{d+1}} \frac{T_i^{3/2}}{m_i^{1/2}} \left(1 - \frac{T_k}{T_i}\right) \left(1 + \frac{m_i T_k}{m_k T_i}\right)^{1/2}, \tag{18}$$

with $k \neq i$.

Note that $\sum_{i=l,s} \mathcal{D}_i^E = 0$, and the *exchange* term $\mathcal{D}_i^E$ is a consequence of the non–equipartition assumption. On the other hand, with the equipartition assumption ($T_l = T_s = T$), $\mathcal{D}_i^E = 0$ and Eq. (17) reduces to:

$$\mathcal{D}_i = \frac{\sqrt{2}d}{\sqrt{\pi}\Omega_d} \sum_j \chi_{ij} R_{ij}^d (1 + R_{ji})^{d-1} M_{ji}^2 (1 - e_{ij}^2) \frac{\phi_i \phi_j}{m_i^{1/2} r_i^{d+1}} \left(\frac{T}{M_{ji}}\right)^{3/2}.$$

2.2.2. Nonequipartition of Granular Energy

It is worthwhile now to comment on the breakdown of the equipartition partition principle for a granular mixture. Physically the lack of energy equipartition is determined by the different dissipation rates (17) and (18). An obvious question is, "How each species will attain a different granular temperature?" The answer to this question depends on the balance between the external power injected into the system and the energy dissipation rates for the two species,[22,24–26] for example, in a vibrofluidized bed.

Before formulating a theory for segregation, it is important to have an estimate of the granular energy ratio T_l/T_s in a fluidized granular mixture. An adequate description of the vibrofluidized granular system requires a careful analysis of the steady version of the species energy balance equations as described above. To formulate the associated boundary-value problem, however, we need to impose appropriate boundary conditions at the base-plate and the free surface of the

vibrofluidized mixture. The problem of boundary conditions to be satisfied for the granular hydrodynamic equations of a vibratory monodisperse system has been studied,[32] but such studies for binary and polydisperse mixtures do not exist. Hence the complete solution of the boundary-value problem for a vibrofluidized mixture is left to a future effort.

In the results presented below, we have rather used the granular energy ratio of Barrat and Trizac[26] which was derived for a randomly heated granular gas (see Section 4). Their expression has subsequently been verified in the molecular dynamics simulations[31] on vibrated granular mixtures. Paolotti *et al.*[31] showed that the granular energy ratio remains constant in the bulk of the mixture, with the variations of T_l/T_s with height being concentrated in two boundary layers near the base plate and the free surface. The experiments[27] also showed the existence of a constant T_l/T_s in the bulk.

3. THEORY OF SEGREGATION

To illustrate how the segregation dynamics can be described by a hydrodynamic approach, we make the following approximations:

- We assume that the granular medium is in a fluidized state. The fluidized state can be realized when the granular material is vibrated strongly in the vertical direction, typically by a harmonic excitation $z_p(t) = A\sin(\omega t)$, with the amplitude A and the frequency $\omega = 2\pi f$. The normalized acceleration parameter ($\Gamma \equiv A\omega^2/\mathrm{g}$) satisfies $\Gamma \gg 1$.
- We assume that the system is in a regime where the bulk-convection and the air-drag can be neglected.
- We neglect the viscous stresses (as well as any stress-anisotropy) for the case where there is no overall mean flow in the system. For example, in a typical experimental realization of a vertically vibrated bed the mean velocity is zero ($\mathbf{u} = \mathbf{0}$).
- We impose horizontal periodic boundary conditions to make the equations analytically tractable. Therefore, the hydrodynamic fields vary only along the vertical direction ($\partial/\partial z(\cdot) \neq 0$, but $\partial/\partial x(\cdot) = 0$ and $\partial/\partial y(\cdot) = 0$).

3.1. Segregation Dynamics: Evolution Equation

Here we outline the derivation of the evolution equation for the Brazil nuts. With the above assumptions, the equations for the evolution of the granular mixture, (1)–(3), (4) and (13), simplify considerably. Our starting point here is the *inviscid* species momentum balance equations (4):

$$\partial_t u_l = -\frac{1}{\varrho_l}\partial_z p_l - \mathrm{g} + \frac{1}{\varrho_l}\Gamma_l, \tag{19}$$

$$\partial_t u_s = -\frac{1}{\varrho_s}\partial_z p_s - \mathrm{g} + \frac{1}{\varrho_s}\Gamma_s. \tag{20}$$

Subtracting Eq. (20) from Eq. (19) we obtain

$$\varrho_l \partial_t u_l^r = -\partial_z p_l + \frac{\varrho_l}{\varrho_s}\partial_z p_s + \left(1 + \frac{\varrho_l}{\varrho_s}\right)\Gamma_l, \tag{21}$$

where $u_l^r = u_l - u_s$ is the relative velocity of the larger particles. Now we need expressions for $\partial_z p_l$ and $\partial_z p_s$.

From the equation of state (6), we define the following weighted-ratio of two partial pressures:[17]

$$\Theta(\phi_i, \phi_i/\phi_j, r_i/r_j, T_i/T_j) = \frac{p_s/n_s}{p_l/n_l} = \frac{p_s}{p_l}\frac{n_l}{n_s},$$

which depends on the species volume fractions, the volume fraction ratio, the size-ratio and the temperature ratio. The partial derivative of p_l is calculated from

$$\partial_z p_l = \frac{\partial}{\partial z}\left(\frac{p_s}{\Theta}\frac{n_l}{n_s}\right) = \frac{p_s}{\Theta}\frac{\partial}{\partial z}\left(\frac{n_l}{n_s}\right) + \frac{n_l}{n_s}\left(\frac{1}{\Theta}\frac{\partial p_s}{\partial z} - \frac{p_s}{\Theta^2}\frac{\partial \Theta}{\partial z}\right).$$

Substituting this in Eq. (21) and using the expression for $\partial_z p_s$ in Eq. (20) (and after some algebraic manipulations), we arrive at the following evolution equation for u_l^r:

$$\begin{aligned}\varrho_l \partial_t u_l^r = {} & n_l\left[m_s\left(\frac{Z_l}{Z_s}\frac{T_l}{T_s}\right) - m_l\right]\mathrm{g} + \left[1 + \frac{n_l}{n_s\Theta}\right]\Gamma_l \\ & - p_l\partial_z\left[\ln\left(\frac{n_l}{n_s\Theta}\right)\right] + n_l\left[m_s\left(\frac{Z_l}{Z_s}\frac{T_l}{T_s}\right) - m_l\right]\partial_t u_s.\end{aligned} \tag{22}$$

In the following we focus on the tracer limit of this equation for a mixture where the number density of intruder (larger) particles is much smaller that of the smaller particles, i.e. $n_l \ll n_s$. In this tracer limit ($n_l \ll n_s$), the intruders are assumed to stay far away from each other (this, of course, implies that larger and smaller particles are homogeneously mixed initially) and they do not influence each-other's motion; in fact, as explained by Lopez de Haro and Cohen,[33] except for the mutual and thermal diffusion coefficients, the transport coefficients of binary mixtures with one tracer component can be obtained from the general expressions of corresponding transport coefficients by taking the limit $n_l/n_s \to 0$.

For analytical simplicity, we make two assumptions: (1) the global temperature of the bed T does not vary with height (see, for example, the experiments in ref. 34); (2) the temperature ratio T_l/T_s remains constant in the bulk which has also been verified in experiments[27] as well as in simulations[31] of vibrated granular mixtures. In the dense collisional regime of a mixture with $n_l \ll n_s$ and $\partial_z T = 0$, the term associated with the momentum exchange in Eq. (22) can be

approximated by:

$$\left(1+\frac{n_l}{n_s\Theta}\right)\Gamma_l \approx \Gamma_l \approx p_l\left(\frac{T_s}{T_l}\right)\left[\partial_z\left(\ln\left(\frac{n_l}{n_s}\right)\right)-\frac{4}{r_{ls}}\left(\frac{2m_lm_s}{\pi m_{ls}T}\right)^{1/2}(u_l-u_s)\right].$$

Furthermore, in this limit, it can be shown that $Z_l/Z_s \approx \phi^2/2$ and hence $\partial_z \ln(Z_lT_l/Z_sT_s) \approx \partial_z \ln\phi^2 = 2\lambda$, where λ is the decay rate of the volume fraction with height: $\ln\phi = \delta + \lambda z$. An approximate value for λ can be estimated from the vibrofluidized experiments:[34] $\lambda r_s < -0.05$ (see Fig. 4c in ref. 34) which is assumed to be valid in the dense regime. Now, the third term on the right-hand side of Eq. (22) and the first term in the above expression can be combined to yield

$$\begin{aligned} &p_l\left(\frac{T_s}{T_l}\right)\partial_z\left[\ln\left(\frac{n_l}{n_s}\right)\right]-p_l\partial_z\left[\ln\left(\frac{n_l}{n_s\Theta}\right)\right]\\ &\quad=p_l\left(\frac{T_s}{T_l}-1\right)\partial_z\left[\ln\left(\frac{\phi_l}{\phi_s}\right)\right]+p_l\partial_z\left[\ln\left(\frac{Z_lT_l}{Z_sT_s}\right)\right]. \end{aligned}$$

Hence, both these terms are of order $O(\lambda p_l)$. With these assumptions and retaining terms of same order in Eq. (22), the time-evolution equation for the relative velocity of intruder particles u_l^r is described by the following equation:

$$\begin{aligned} m_l\frac{\mathrm{d}u_l^r}{\mathrm{d}t} &= \left[m_s\left(\frac{Z_l}{Z_s}\frac{T_l}{T_s}\right)-m_l\right]\mathrm{g}-\frac{4K_{ls}T}{r_{ls}}\left(\frac{2m_lm_s}{\pi m_{ls}T}\right)^{1/2}u_l^r\\ &\quad+\left[m_s\left(\frac{Z_l}{Z_s}\frac{T_l}{T_s}\right)-m_l\right]\frac{\mathrm{d}u_s}{\mathrm{d}t}, \end{aligned} \tag{23}$$

where all expressions are evaluated in the limit $n_l/n_s \to 0$.

The above equation (23) contains all the information necessary to describe the segregation dynamics of intruders in the tracer limit. The first term on the right hand side is the net gravitational force acting on the intruder. Note that the second term has a form similar to the Stokes' drag force, which always acts opposite to the intruder's movement. The functional form of this term can be justified by recalling the experimental observations of Zik *et al.*,[35] who found a linear dependence of the drag force on the velocity of a sphere moving in a vibrofluidized granular medium. This could be interpreted as a characteristic of the fluidized state of the granular media. The last term represents a weighted *coupling* with the inertia of the smaller particles. In the following subsection, we discuss the origin of these forces in detail.

3.2. Segregation Forces

Let us now analyse different forces that are acting on the intruder as it rises/sinks through the granular bed.

3.2.1. Gravitational Forces: Buoyancy and Geometric Forces

We can decompose the net gravitational force in Eq. (23) on an intruder in the following manner:

$$F = \mathrm{g}\left[(\rho_s - \rho_l)V_l + m_s\left(\frac{T_l}{T_s} - 1\right)\frac{Z_l}{Z_s} + m_s\left(1 - \frac{V_l}{V_s}\right) + m_s\left(\frac{Z_l}{Z_s} - 1\right)\right], \tag{24}$$

where V_i is the volume of a particle of species i. This net gravitational force is composed of the following *buoyant* and *geometrical* forces:

- An *Archimedean buoyancy* force due to the weight of the displaced volume of the intruder (V_l):

$$F_b^A := V_l(\rho_s - \rho_l)\mathrm{g}. \tag{25}$$

- An analogue of the *thermal buoyancy* force due to the difference between the two granular temperatures:

$$F_b^T := \beta(T_l - T_s), \tag{26}$$

  where $\beta = m_s T_s^{-1}(Z_l/Z_s)$ is the effective pseudo-thermal expansion coefficient. We call this *pseudo-thermal buoyancy* force. Note that this force vanishes identically for a mixture of particles with elastic collisions ($e_{ij} = 1$).
- Due to the size–disparity between the intruder and the smaller particles, the intruder has to overcome a compressive volumetric strain, $\epsilon_v^{\mathrm{st}} := (V_l/V_s - 1)$. This results in a *static compressive* force of the form:

$$F_{\mathrm{ge}}^{\mathrm{st}} := -m_s \mathrm{g}\epsilon_v^{\mathrm{st}}, \tag{27}$$

  This force is always negative since the intruder has to rise against gravity.
- A *dynamic tensile* force from the pressure difference due to the interaction between the intruder and the smaller particles:

$$F_{\mathrm{ge}}^{\mathrm{dyn}} := m_s \mathrm{g}\epsilon_v^{\mathrm{dyn}}, \tag{28}$$

  where $\epsilon_v^{\mathrm{dyn}} := (Z_l/Z_s - 1) \geq 0$ can be associated with a weighted *volumetric* strain, *tensile* in nature.

The last two forces (27) and (28) are not related to standard buoyancy arguments. Thus, purely *geometric* effects due to the *size-disparity* contribute two new types of segregation forces:

$$F_{\mathrm{ge}} = F_{\mathrm{ge}}^{\mathrm{st}} + F_{\mathrm{ge}}^{\mathrm{dyn}} = -m_s\left(\epsilon_v^{\mathrm{st}} - \epsilon_v^{\mathrm{dyn}}\right)\mathrm{g}. \tag{29}$$

Overall, the collisional interactions help to reduce the net compressive force that the intruder has to overcome.

It is interesting to find out whether we could get back the standard Archimedes law from Eq. (24). This corresponds to the case where a large particle is immersed in a sea of small particles with $r_l \gg r_s$. For this limit, it follows that[19]

$$F_{\rm ge}^{\rm dyn} \to m_s(V_l/V_s - 1) = -F_{\rm ge}^{\rm st} \tag{30}$$

and the net geometric force is

$$F_{\rm ge} \equiv 0. \tag{31}$$

Thus, the net gravitational force on a particle falling/rising in an otherwise quiscent fluid (at the same temperature) boils down to the Archimedean buoyancy force:

$$F = F_B^A = {\rm g}(\rho_s - \rho_l)V_l. \tag{32}$$

3.2.2. Unsteady Forces: The Added Mass Effect

We have noted in the previous section that the inertia of the smaller particles is directly coupled with the motion of the intruder in the evolution equation (viz. Eq. 23). For this unsteady (inertial) force ${}^tF$ also, we follow our earlier decomposition:

$$\begin{aligned} {}^tF = \frac{{\rm d}u_s}{{\rm d}t}\Bigg[&(\rho_s - \rho_l)V_l + m_s\left(\frac{T_l}{T_s} - 1\right)\frac{Z_l}{Z_s} \\ &+ m_s\left(1 - \frac{V_l}{V_s}\right) + m_s\left(\frac{Z_l}{Z_s} - 1\right)\Bigg]. \end{aligned} \tag{33}$$

It is evident now that the net unsteady term has contributions from the standard *added mass force* along with two new forces as described below.

- As in the unsteady-motion of a particle in a fluid, the intruder in a granular mixture has to rise along with its surrounding smaller particles. The 'added' inertia of the displaced smaller particles that are being carried by the intruder gives rise to an effective *added mass force*[36] on the intruder:

$${}^tF_{am} = V_l(\rho_s - \rho_l)\frac{{\rm d}u_s}{{\rm d}t}. \tag{34}$$

  As expected, this force vanishes if the material density of the intruder is the same as that of smaller particles.
- A thermal analog to the *added mass force*, due to the difference between the two granular temperatures, is given by:

$${}^tF_{am}^T = m_s\frac{Z_l}{Z_s}\left(\frac{T_l}{T_s} - 1\right)\frac{{\rm d}u_s}{{\rm d}t}. \tag{35}$$

This force vanishes identically for $T_l = T_s$ that holds if the particle collisions are perfectly *elastic*. Hence this represents a *new* force for the granular system.

- Lastly, we have exact analogues of the two geometric forces as described in the previous section:

$$ {}^{t}F_{am}^{ge} = m_s \left(1 - \frac{V_l}{V_s}\right) \frac{\mathrm{d}u_s}{\mathrm{d}t} = -m_s \epsilon_v^{\mathrm{st}} \frac{\mathrm{d}u_s}{\mathrm{d}t}. \tag{36} $$

$$ {}^{t}F_{am}^{ge} = m_s \left(\frac{Z_l}{Z_s} - 1\right) \frac{\mathrm{d}u_s}{\mathrm{d}t} = m_s \epsilon_v^{\mathrm{dyn}} \frac{\mathrm{d}u_s}{\mathrm{d}t}. \tag{37} $$

While the former is the analog of static 'compressive' geometric force, the latter is the analog of the dynamic 'tensile' geometric force as discussed in the previous section. Both these forces vanish if the intruder is of the same size as the bed-materials.

Thus, we have shown that the last term in the evolution equation (23) can be represented by an weighted *added-mass force*.

4. PHASE DIAGRAM FOR BNP/RBNP TRANSITION AND THE REVERSE BUOYANCY EFFECT

To proceed in the simplest possible way, we first consider the *steady-state* solution of equation (23)– in this case the added-mass forces do not influence the *onset* of segregation. Neglecting transient effects, the steady relative velocity of the intruder can be obtained from

$$ u_l^r = \frac{r_{ls}\mathrm{g}}{4K_{ls}} \left(\frac{\pi m_{ls}}{2m_l m_s T}\right)^{1/2} \left[m_s \left(\frac{Z_l}{Z_s}\frac{T_l}{T_s}\right) - m_l\right]. \tag{38} $$

Setting this relative velocity to zero, we obtain the criterion for the *transition* from BNP to RBNP:

$$ m_s \left(\frac{Z_l}{Z_s}\frac{T_l}{T_s}\right) - m_l = 0, \tag{39} $$

which agrees with the expression of Jenkins and Yoon[17] for the case of equal granular energies ($T_l = T_s$), i.e. $Z_l/Z_s = m_l/m_s$. We have already noted in our previous paper [19] that the non-equipartition of granular energy ($T_l \neq T_s$) that arises from the dissipative nature of particle collisions must be incorporated into the theory to correctly describe many experimental findings.

As mentioned before, the energy ratio, $R_T = T_l/T_s$, is calculated from the model of Barrat and Trizac:[26]

$$C_1 R_T^{3/2} + C_2 \left(1 + \frac{m_s}{m_l} R_T\right)^{3/2} + C_3 \left(1 + \frac{m_s}{m_l} R_T\right)^{1/2} (R_T - 1) + C_4 = 0, \tag{40}$$

where

$$\begin{aligned}
C_1 &= 2^{d-1}\left(1 - e_{ll}^2\right)\phi_l R_{sl}^d \chi_{ll} \left(\frac{m_s}{m_l}\right)^{3/2}, \\
C_2 &= \sqrt{2}\left(1 - e_{ls}^2\right)(1 + R_{sl})^{d-1} \left(\phi_s M_{sl}^2, -\phi_l R_{sl}^d M_{ls}^2\right) \chi_{ls}, \\
C_3 &= 2\sqrt{2}(1 + e_{ls})(1 + R_{sl})^{d-1} M_{sl} \left(\phi_s M_{sl} + \phi_l R_{sl}^d M_{ls}\right) \chi_{ls}, \\
C_4 &= -2^{d-1}\left(1 - e_{ss}^2\right)\phi_s R_{sl}^{d-1} \chi_{ss}.
\end{aligned}$$

To draw the phase-diagram in the $(m_l/m_s, r_l/r_s)$-plane, we need to solve the segregation criterion (39) in conjunction with the expresion for T_l/T_s (40). This leads to a quadratic polynomial for the mass-ratio m_l/m_s, resulting in *multivaluedness* for m_l/m_s below a critical value of the size-ratio r_l/r_s as we discuss in the following. We note that another choice of T_l/T_s, as suggested by one of the referees, does not change the qualitative nature of our results.

In Fig. 1 we plot the phase diagram for the BNP/RBNP transition for a mixture of spheres in the tracer limit ($\phi_l/\phi_s = 10^{-8}$) at a total volume fraction of $\phi = 0.5$. Note that this volume fraction is well below the value that corresponds to the perfect cubic-packing ($\phi = \pi/6 \approx 0.52$), implying that the mixture is in the 'liquid' regime. Each solid curve in Fig. 1, for a specified restitution coefficient, demarcates the zones of BNP and RBNP transition. We observe that the qualitative nature of the phase-diagram changes even if the particles are *slightly* inelastic ($e = 0.99$); for example, the mass-ratio (m_l/m_s) is a *multi-valued* function of the size-ratio for $e \neq 1$, in contrast to the perfectly elastic case (denoted by the dashed line). The effect of dissipation is to introduce a *threshold size-ratio* above which there is no RBNP. Moreover, the zone of RBNP shrinks dramatically when the particles are more dissipative; for this parameter combination, there is no reverse segregation for moderately dissipative particles $e < 0.8$. We shall come back to discuss this point in the next subsection in connection with the reverse-buoyancy effect.[10]

As discussed in our previous paper,[19] we need to look at various segregation forces to understand the driving mechanism for BNP/RBNP transition. First, we focus our attention to a mixture of equal density particles ($\rho_l = \rho_s$); this case is easily amenable to experiments by using the intruder and the smaller particles of the same material.

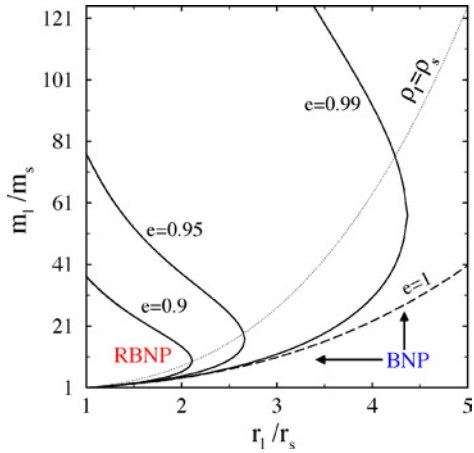

Fig. 1. (color online) Effect of inelasticity on the phase diagram for BNP/RBNP in three dimensions: $\phi = 0.5$ and $\phi_l/\phi_s = 10^{-8}$. The dotted line represents a mixture of equal density particles ($\rho_l = \rho_s$): $m_l/m_s = (r_l/r_s)^3$.

For an equal density mixture, the variations of different segregation forces with the size-ratio are plotted in Fig. 2. The coefficient of restitution is set to 0.95. Since $\rho_l = \rho_s$, the Archimedean buoyancy force, $F_b^A \propto (\rho_l - \rho_s)$, is identically zero as shown by the dotted horizontal line in Fig. 2. The upper inset in Fig. 2 shows the variations of two geometric forces, and the net geometric force, $F_{\rm ge}$, is *negative* as shown by the dot-dash line. However, the pseudo-thermal buoyancy force, $F_b^T \propto (T_l - T_s)$, is positive and increases with increasing size-ratio. Thus, the net gravitational force, $F = F_b + F_{\rm ge} \equiv F_b^T + F_{\rm ge}$, can be positive/negative when F_b^T greater/less than $F_{\rm ge}$, respectively, with the equality being the BNP/RBNP transition point. The solid line in Fig. 2 shows the variation of the net gravitational force F that changes sign at a size-ratio of $r_l/r_s \approx 2.6$ above which the intruder rises (BNP) and below which it sinks (RBNP). Clearly, this *threshold size-ratio* is decided by a competition between the buoyancy forces and the geometric forces, leading to the onset of BNP/RBNP transition.[19] Note that for a mixture of particles with elastic collisions ($e = 1$), the pseudo-thermal buoyancy force is $F_b^T = 0$ and hence $F \equiv F_{\rm ge} < 0$; the intruder in such a mixture will, therefore, sink for the parameter combinations of Figs. 1 and 2.

Now we focus on a mixture with the mass-ratio, m_l/m_s, between the intruder and the bed-particles being fixed; this can be realized in experiments by fixing the bed materials (glass beads or steel balls, etc.) and subsequently by varying the size and the density of the intruder. The variation of segregation forces with the size-ratio is shown in Fig. 3 for $m_l/m_s = 10$; other parameters are as in Fig. 1. Both the buoyancy and geometric forces are negative at $R_{ls} = 1$ as seen in Fig. 3a.

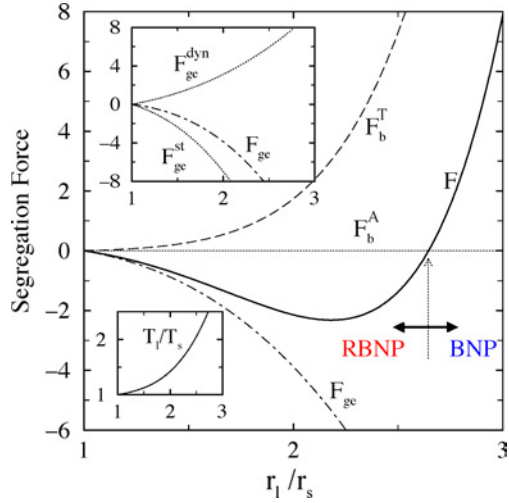

Fig. 2. (color online) Variations of segregation forces ($F/m_s g$) with the size-ratio for a mixture of equal-density particles ($\rho_l = \rho_s$) at $e = 0.95$. The dotted arrow indicates the locus of the transition BNP $\Leftrightarrow$ RBNP. The upper inset shows the variations of the static and dynamic contributions to the total geometric force ($F_{\rm ge} = F^{\rm st}_{\rm ge} + F^{\rm dyn}_{\rm ge}$) with the size-ratio. The lower inset shows the variation of T_l/T_s with the size-ratio.[26]

While the net buoyancy force increases with the size-ratio, the net geometric force decreases in the same limit, and again the competition between these two forces decides the onset of BNP/RBNP. We observe in Fig. 3b that the pseudo-thermal buoyancy force F_b^T remains positive only upto a size-ratio of $R_{ls} \leq 11.8$ and becomes negative thereafter (this is a consequence of the energy-ratio T_l/T_s being less than 1 for $R_{ls} > 11.8$, see inset in Fig. 3b). For this mixture, however, the Archimedean buoyancy force overwhelms its pseudo-thermal counterpart (i.e. $F_b^A \gg F_b^T$) beyond a moderate size-ratio of $R_{ls} > 3$. Hence, it is the competition between the Archimedean buoyancy force and the geometric forces that mainly determines the *threshold size-ratio* for the BNP/RBNP transition ($R_{ls} \approx 2.5$) for this case.

4.1. Reverse Buoyancy and Beyond

In 1998 Shinbrot and Muzzio[10] discovered an interesting effect: even though large heavy intruders can rise to the top in a vibrofluidized mixture of smaller particles, relatively *lighter* intruders of the same size can sink to the bottom. This is in contradiction to common expectation and has been appropriately dubbed the *reverse buoyancy effect*. (Strictly speaking, however, the rising-phenomenon of 'heavier' intruders is also a reverse-buoyancy effect.) In the following we refer to

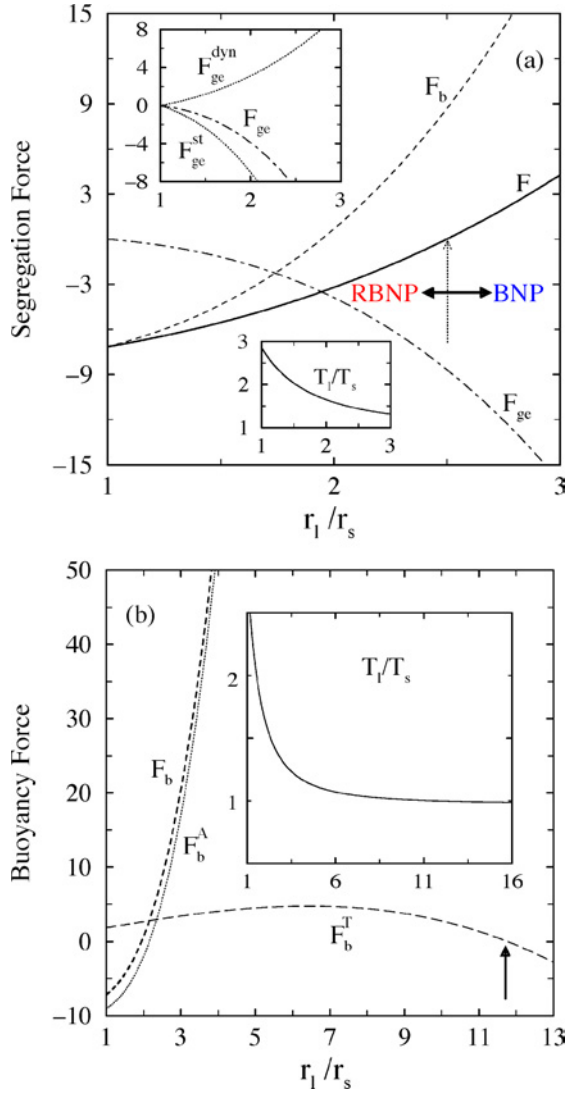

Fig. 3. (color online) (a) Variations of segregation forces ($F/m_s g$) with the size-ratio for a mixture with fixed mass-ratio ($m_l/m_s = 10$) at $e = 0.95$. The dotted arrow indicates the locus of the transition BNP $\Leftrightarrow$ RBNP. The upper inset shows the variations of the static and dynamic contributions to the total geometric force ($F_{\rm ge} = F_{\rm ge}^{\rm st} + F_{\rm ge}^{\rm dyn}$) with the size-ratio. The lower inset shows the variation of T_l/T_s with the size-ratio. (b) Variations of Archimidean (F_b^A) and thermal (F_b^T) buoyancy forces with r_l/r_s, with parameter values as in (a). The arrow on the F_b^T-curve indicates the size-ratio above which $F_b^T < 0$.

the sinking-phenomenon of 'lighter' intruders ($\rho_l/\rho_s < 1$) as the reverse-buoyancy effect as in Shinbrot and Muzzio.

To explore whether our model is able to explain this effect or not, we have fixed the size-ratio at $R_{ls} = 2.5$, and changed the mass-ratio by varying the density-ratio; again this can be realized in experiments by varying the material density of either the intruder or the smaller particles. Figure 4a shows the onset of the *reverse buoyancy effect* where we have plotted the variations of different segregation forces with the mass-ratio, m_l/m_s, with other parameter values as in Fig. 2. To contrast the mass-ratio and density-ratio effects simultaneously, the same figure is redrawn in Fig. 4b, with the abscissa now representing the density-ratio, ρ_l/ρ_s. For a fixed size-ratio, the net geometric force remains constant as shown by the dot-dash line in Fig. 4. The upper inset in Fig. 4 shows the Archimedean and pseudo-thermal contributions to the total buoyancy force; while F_b^T increases with the mass-ratio, F_b^A decreases in the same limit, and the total buoyancy force varies *non-monotonically* with both mass- and density-ratios.

Focussing on the mass-ratio of $m_l/m_s = 30$ (the density-ratio is $\rho_l/\rho_s \approx 1.98$) in Fig. 4, we note that the net gravitational force is positive, i.e. the heavier intruder will rise to the top (which is the BNP). Looking at the upper inset in Fig. 4a, we find that it is the pseudo-thermal buoyancy force that drives the intruder to the top (at such large density-ratios). Now if we decrease the mass of the intruder (by decreasing its material density ρ_l) to $m_l/m_s \approx 25$ (that corresponds to a density-ratio of $\rho_l/\rho_s \approx 1.6$), the net gravitational force becomes negative. Hence this relatively *lighter* intruder ($\rho_l/\rho_s < 1.6$) will now sink to the bottom (i.e. which is the RBNP). When we lower the density-ratio even below unity, the lighter intruder sinks to the bottom as observed in Fig. 4b. This is nothing but the reverse-buoyancy effect of Shinbrot and Muzzio:[10] *although the heavier intruder can rise to the top, equally large but a relatively lighter intruder can sink.*

It is interesting to observe in Fig. 4 that there is a window of mass- and density-ratios ($10 < m_l/m_s < 25$ and $0.64 < \rho_l/\rho_s < 1.6$) for which the net gravitational force remains negative and hence the intruder will sink. For $\rho_l/\rho_s < 0.64$, however, the Archimedean buoyancy force prevails over other forces and the lighter intruder rises to the top (as observed in the upper inset of Fig. 4b). This implies that if the material density of the intruder is much less than that of the bed particles, the intruder will eventually show the standard buoyancy effect (which is again the BNP).

To understand the origin of reverse buoyancy, we consider particles with perfectly elastic collisions ($e = 1$), for which $T_l = T_s$ and $F_b^T = 0$; hence the net gravitational force, $F \equiv F_b^A + F_{\rm ge}$, will decrease monotonically with increasing size-ratio as shown by the red-line in the lower inset of Fig. 4b. In such a mixture of elastic particles, an intruder with $R_{\rho 1} = \rho_l/\rho_s > 0.44$ will sink (i.e. the reverse buoyancy), and this *threshold density-ratio* is less than unity since the lighter intruder has to overcome the net *compressive* geometric force. Thus, *the onset of*

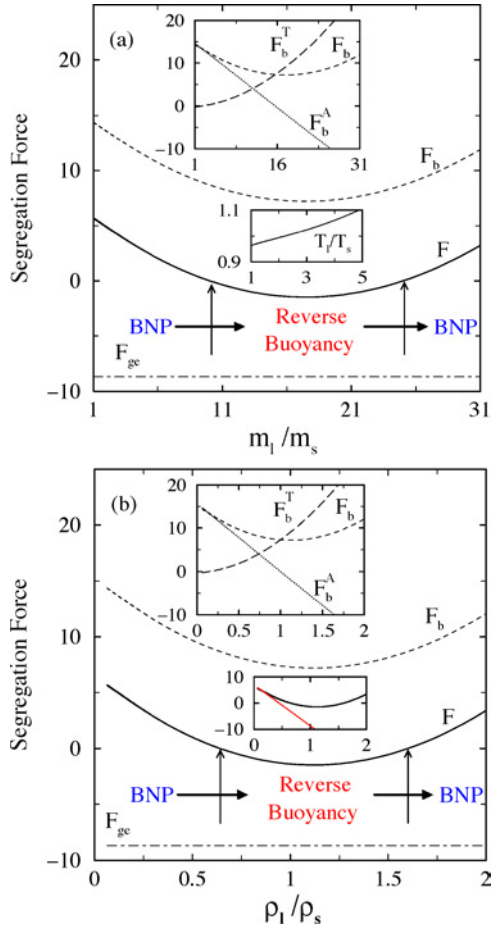

Fig. 4. (color online) (a) Onset of *reverse buoyancy effect* in terms of segregation forces: variations of $F/m_s g$ with the mass-ratio for a mixture with $r_l/r_s = 2.5$. Parameter values are $\phi = 0.5, \phi_l/\phi_s = 10^{-8}$ and $e = 0.95$. The vertical arrows indicate the loci of the transition BNP $\Leftrightarrow$ RBNP. The upper inset shows the variations of the Archimedean and pseudo-thermal contributions to the total buoyancy force ($F_b = F_b^A + F_b^T$) with the mass-ratio. The lower inset shows the variation of T_l/T_s with the mass-ratio. (b) Same as in *a* but with density-ratio, ρ_l/ρ_s. The redline in the lower inset shows the variation of $F_b^A + F_{\rm ge}$.

reverse buoyancy results from a competition between the Archimedean buoyancy force and the net compressive geometric force.

The effect of the pseudo-thermal buoyancy force (for dissipative particles) is simply to increase this threshold density-ratio to $R_{\rho 1} \approx 0.64$ for parameter combinations of Fig. 4, and create another threshold density-ratio at $R_{\rho 2} \approx 1.6$,

above unity, beyond which the heavier intruder rises to the top (i.e. BNP). Thus, the lower threshold density-ratio $R_{\rho 1}$ is created by the geometric forces and the higher threshold density-ratio $R_{\rho 2}$ is created by the pseudo-thermal buoyancy force.

It is interesting to point out that the threshold density-ratio $R_{\rho 2}$ at which the RBNP occurs depends crucially on the overall mean volume fraction (that can be related with the shaking strength of the vibrator, see Section 4.2) of the fluidized bed. For example, by reducing the mean volume fraction, $R_{\rho 2}$ can be pushed below unity.

Thus, our model predicts that the intruder will show the BNP for $\rho_l/\rho_s \gg 1$ and $\rho_l/\rho_s \ll 1$. While the BNP in the former limit is driven by the pseudo-thermal buoyancy force, the BNP in the latter limit is driven by the Archimedean buoyancy force. For intermideate values of density-ratios, the intruder will show the RBNP (and the reverse buoyancy) which is driven by a competition between the buoyancy and geometric forces.

Now we make a few comments on the experimental realizations of reverse buoyancy. The range of size-ratios for which our model predicts the reverse buoyancy effect is of order $R_{ls} = O(5)$ for the coefficient of restitution $e < 0.99$; for larger values of R_{ls} our model predictions show the standard Brazil-nut segregation. However, this critical size-ratio can be pushed to a much higher value by considering higher values of e; this is equivalent to reducing the magnitude of the pseudo-thermal buoyancy (F_b^T), since F_b^T vanishes as the energy ratio T_l/T_s approaches its equipartition value for perfectly elastic system ($e = 1$).

More recently, Yan *et al.*[37] have also observed the reverse buoyancy effect for a range of size-ratios varying between 25 to 36; the diameter of their bed-particles was less than 250 μm. Interestingly, the critical density at which this transition ocurred was $R_{\rho 2} = \rho_l/\rho_s \approx 0.7$. But the interstitial air-pressure has played a crucial role in their experiments since *they could not observe RBNP when the experiments were performed at a reduced air-pressure* (0.1 atm). Thus, the missing link could be provided by the *air-drag* that we have neglected in our analysis.

Our predictions of a transition to BNP for very light intruders (at $R_\rho \ll R_{\rho 1}$) has been recently observed by Huerta and Ruiz-Suarez.[39] Their experiments at high frequencies ($f = 50$ Hz and $\Gamma = 3$) would closely mimic most of our assumptions since bulk-convection was negligible in their experiments. More careful experiments at vacuum are needed to map out the whole phase-diagram.

4.2. Effect of Shaking Strength

Here we consider the effect of the shaking strength of vibration on the BNP/RBNP transition. In typical vibrofluidized-bed experiments, the mixture is

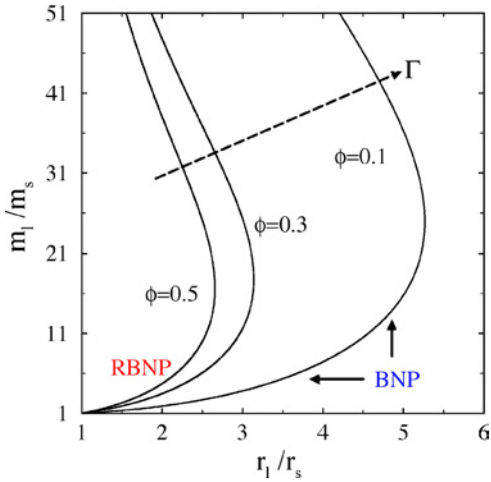

Fig. 5. (color online) Effect of mean volume fraction on the phase diagrams for BNP/RBNP in three dimensions: $e = 0.95$ and $\phi_l/\phi_s = 10^{-8}$. The dashed arrow indicates the direction of increasing shaking strength Γ.

vibrated via a sinusoidal excitation of the base-plate:

$$z_p(t) = A\sin(2\pi f t), \tag{41}$$

where A is the amplitude of vibration and f is its frequency. The shaking strength of vibration can be measured via the following non-dimensional number

$$\Gamma = \frac{A(2\pi f)^2}{g}. \tag{42}$$

Ideally, the fluidized regime corresponds to both large-amplitude and high-frequency vibrations which can be related to the case $\Gamma \gg 1$. Note that this condition, $\Gamma \gg 1$, can be realized either by increasing the shaking amplitude at fixed f or by increasing the shaking frequency at fixed A.

In the fluidized-regime, the bed expands with increasing shaking strength Γ, leading to a decrease in the overall volume fraction of the mixture ϕ. Thus, the effect of Γ on the phase-diagram for BNP/RBNP can be tied to the effect of varying the mixture volume fraction ϕ. This is shown in Fig. 5 where we have plotted three curves for different volume fractions ($\phi = 0.1, 0.3, 0.5$) with $\phi_l/\phi_s = 10^{-8}$. We observe that the range of size- and mass-ratios, for which the RBNP exists, increases with decreasing ϕ. This implies that the possibility of RBNP will increase with increasing shaking strength Γ. The experimental findings of Breu *et al.*[13] showed similar trends with Γ, which our model is able to mimic.

To understand the effect of mean volume fraction on the BNP/RBNP transition, we analyse different segregation forces for a given size-ratio and mass-ratio

(say, at $r_l/r_s = 4$ and $m_l/m_s = 40$ in Fig. 5). For this, both the Archimedean buoyancy force F_b^A and the static geometric force $F_{\rm ge}^{\rm st}$ do not vary with ϕ. The dynamic geometric force $F_{\rm ge}^{\rm dyn}$, however, decreases with decreasing ϕ. In this limit, the collision frequency decreases that decreases the collisional pressure, and hence the intruder will become relatively less mobile. For this case, even though the granular energy ratio do not vary appreciably with ϕ, the pseudo-thermal buoyancy force F_b^T will decrease with ϕ as a result of a decrease in the value of Z_l/Z_s. Both these effects result in a lower value of the 'upward' force on the intruder and hence the intruder will show the RBNP with decreasing mean volume fraction (i.e. with increasing shaking strength). For these parameter conditions, the mean density at which the BNP/RBNP transition occurs is about 0.284.

4.3. Effect of Intruder Volume Fraction

So far we have shown results for a binary mixture in the tracer limit of intruders (i.e. $\phi_l/\phi_s = 10^{-8}$). Recall from Fig. 1 that the zone of RBNP shrinks to zero as we make the particles more and more dissipative since the pseudo-thermal buoyancy force increases in the same limit. Hence, the RBNP is unlikely to occur in the tracer limit for moderately dissipative particles.

To probe the effect of the volume fraction of the intruders, we show the phase-diagram for the BNP/RBNP transition in Fig. 6 for three relative volume

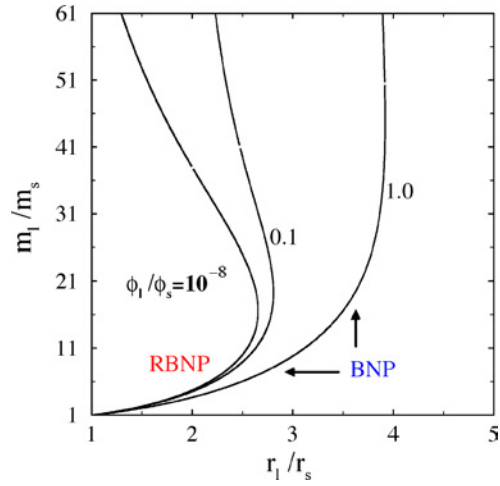

Fig. 6. (color online) Effect of the relative volume fraction of intruders on the phase diagram for BNP/RBNP in three dimensions: $\phi = 0.5$ and $e = 0.95$.

fractions: $\phi_l/\phi_s = 10^{-8}$, 0.1 and 1. The other parameters are as in Fig. 2. As we increase the relative volume fraction of the intruders, the ranges of mass- and size-ratios for which the reverse segregation (RBNP) occurs increase sharply. It is interesting to recall that most of the experiments of Breu *et al.*[13] correspond to the case where the number of layers of each species was equal; this translates into $\phi_l > \phi_s$. However, when they *reduced the number density of larger particles they could not observe RBNP* (with other conditions remaining the same). Also, the recent experiments of Yan *et al.*[37] (at reduced air-pressures) do not show RBNP. Our model predictions are, therefore, in qualitative agreement with these experimental findings. Clearly, more experiments are needed to map out the correct phase-diagram for various volume fractions of the intruders.

5. DYNAMICS OF INTRUDERS IN TRACER LIMIT: NONMONOTONIC RISE TIME

As an application of our theoretical framework, we now consider the dynamics of intruders in the tracer limit ($n_l \ll n_s$) and determine the intruder's relative velocity u_l^r and its *rise-time*. (Hereafter, the dynamics of intruder particles in the tracer limit is considered to be that of a single intruder in a bed of small particles.) Note that these two quantities have been measured[5,6,39] in many Brazil-nut experiments.

To probe the motion of the intruder, we need to know the macroscopic velocity-field u_s of the smaller particles *a priori*. Let the system be excited by a periodic force in the vertical direction with a (symmetric) harmonic displacement: $z_p(t) = A\sin(\omega t)$. We assume that the vibrofluidized state of the smaller particles is coupled to this periodic movement, and make the following approximation for the velocity u_s of the smaller particles:

$$u_s \approx \frac{\mathrm{d}z_p}{\mathrm{d}t} = -A\omega\cos(\omega t). \tag{43}$$

This simply implies that the smaller particles follow the motion of the base plate which is a reasonable assumption for shakings at *a high frequency but with low amplitudes* ($\Gamma \gg 1$).

We need to estimate the granular temperature of the mixture T which appears in the drag term in the evolution equation (23). In the tracer limit ($n_l \ll n_s$), the mixture granular temperature would be that of an equivalent monodisperse system of smaller particles;[33] we have already assumed that the granular temperature is uniform throughout the bed. Considering this homogeneous-state of fluidization, the global temperature can be estimated by equating the rate of energy input through the bottom plate with the rate of energy loss due to inelastic particle

collisions:[38]

$$T = \frac{1}{\sqrt{2}\pi}\frac{m_s S_p}{N r_s^2}\frac{(A\omega)^2}{(1-e_{ss}^2)}. \tag{44}$$

Here S_p is the surface area of the base-plate and N is the total number of particles. As demonstrated in many earlier studies, this provides a reasonable approximation for the average temperature of the bed, and represents the leading-order solution even in the dense limit.[38] We assume that in the fluidized state the height of the bed is H. Thus, the expression for the global temperature can be rewritten as

$$T = \frac{\sqrt{2}}{3}\frac{m_s A^2\omega^2}{\phi_s R_H R_{ls}(1-e_{ss}^2)}. \tag{45}$$

where

$$R_H = \frac{H}{2r_l} \tag{46}$$

is the non-dimensional bed-height as a multiple of the intruder-diameter, and $R_{ls} = r_l/r_s$ the size-ratio.

Let us introduce the following reference scales for non-dimensionalization:

$$\left.\begin{aligned} \overline{u}_l^r &= \frac{u_l^r}{u_R} = \frac{u_l^r}{A\omega} \\ \overline{T} &= \frac{T}{T_R} = \frac{T}{m_s A^2\omega^2} \\ \overline{t} &= \frac{t}{t_R} = \frac{t}{\omega^{-1}} \end{aligned}\right\} \tag{47}$$

where the quantities with overbars are non-dimensional. Hereafter, for convenience, we will drop the overbar on the non-dimensional quantities. With this scaling, the non-dimensional granular temperature has the following expression:

$$T = \frac{\sqrt{2}}{3\phi_s R_H R_{ls}(1-e_{ss}^2)}. \tag{48}$$

The evolution equation (23) in non-dimensional form can now be written as

$$\frac{\mathrm{d}u_l^r}{\mathrm{d}t} = \alpha(\Gamma^{-1} - \sin t) - \beta u_l^r \tag{49}$$

where

$$\beta = \beta_0 R_A\sqrt{T} \tag{50}$$

is the non-dimensional drag coefficient which is a function of the bed-temperature T and the amplitude of the harmonic-shaking

$$R_A = \frac{A}{2r_l}. \tag{51}$$

Here α and β_0 are non-dimensional functions of the size-ratio, mass-ratio and volume fraction:

$$\alpha = \left(\frac{m_s}{m_l}\frac{Z_l}{Z_s}\frac{T_l}{T_s} - 1\right)$$

$$\beta_0 = 8K_{ls}\left(\frac{R_{ls}}{R_{ls}+1}\right)\left(\frac{2}{\pi}\frac{m_s}{m_l}M_{sl}\right)^{1/2}$$

$$K_{ls} = \frac{1}{4}\phi_s\chi_{ls}(1+R_{ls})^3$$

$$M_{sl} = \frac{m_s}{m_l+m_s}$$

$$R_{ls} = \frac{r_l}{r_s}.$$

The solution to the differential equation (49), with initial condition $u_l^r(t)|_{t=0} = 0$, is given by

$$u_l^r(t) = \frac{\alpha}{\beta\Gamma}(1-e^{-\beta t}) - \left(\frac{\alpha}{1+\beta^2}\right)(e^{-\beta t} - \cos t + \beta\sin t). \tag{52}$$

The temporal evolution of the position of the intruder, $z_l(t)$, can be obtained by integrating Eq. (52):

$$z_l(t) = \frac{\alpha R_A}{\beta^2\Gamma}(\beta t + e^{-\beta t}) - \frac{\alpha R_A}{\beta^2\Gamma}(1+\beta\Gamma) + z_0$$
$$+ \left(\frac{\alpha R_A}{\beta(1+\beta^2)}\right)(e^{-\beta t} + \beta\sin t + \beta^2\cos t) \tag{53}$$

with $z_0 \equiv z_l(0)$ being the position of the intruder at time $t = 0$. Note that z_l has been non-dimensionalized by the diameter of the intruder.

5.1. Rise Time: Non-monotonicity and Experiments

By knowing the steady relative velocity of the intruder u_l^r, we can calculate its *rise-time* τ:

$$\tau = \frac{2r_l}{u_l^r} = \frac{2r_l\beta\Gamma}{\alpha}. \tag{54}$$

This is the (non-dimensional) time that the intruder will take to travel a height of one intruder diameter. In the following we have plotted the rise-time in cycles.

First, we consider an intruder of a given size-ratio ($R_{ls} = r_l/r_s = 2.5$) and vary its density; further, we assume the equipartition assumption $T_l = T_s$. For this case, the variation of the rise-time with the density-ratio, $R_\rho = \rho_l/\rho_s$, is shown in

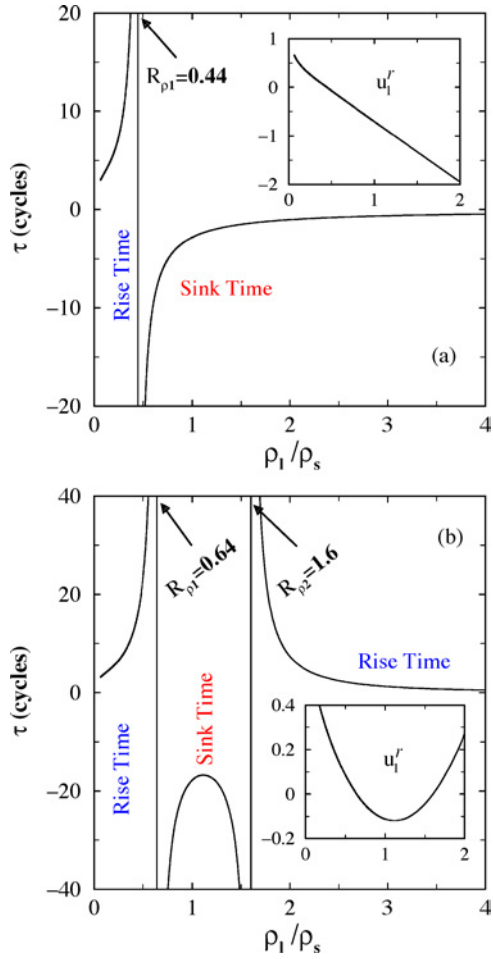

Fig. 7. (color online) (a) Variations of rise (/sink) time τ (in cycles) with density-ratio for $T_l = T_s$; the parameter values are as in Fig. 4. The shaking parameters are $\Gamma = 5$, $f = 50$ Hz; the intruder diameter is 4.97 cm and the bed-height $R_H = H/(2r_l) = 10$. (b) Same as *a* with non-equipartition assumption. The inset in each panel shows the variation of the intruder's relative velocity, u_l^r, with the density-ratio. The vertical lines in each panel refer to density-ratios for the *BNP/RBNP* transition.

Fig. 7a; other parameters are as in Fig. 4. The parameters for base-plate excitations are $\Gamma = 5$ and $f = 50$ Hz; we set the bed-height to $R_H = H/(2r_l) = 10$. As expected, τ diverges at the onset of BNP/RBNP ($R_{\rho 1} \approx 0.64$) since the intruder velocity, u_l^r changes its sign at this threshold density as seen in the inset of Fig. 7a. For $R_\rho > R_{\rho 1}$, the sink-time decreases, implying that the heavier intruders sink faster; for $R_\rho < R_{\rho 1}$, the lighter intruders rise faster.

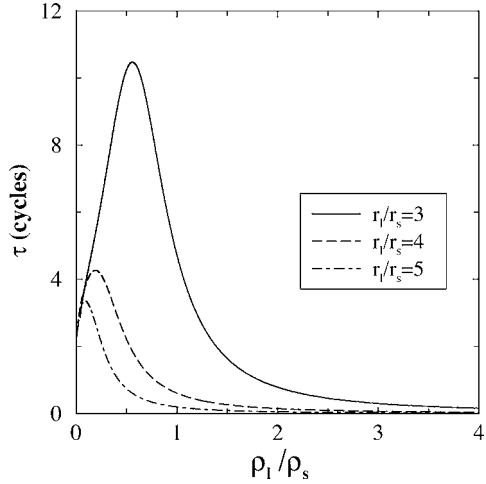

Fig. 8. Variation of rise time τ (in cycles) with density-ratio for different size-ratios; the parameter values are as in Fig. 5. The shaking parameters are as in Fig. 7.

Now we relax the equipartition assumption, i.e. $T_l \neq T_s$, and plot the variation of τ with R_ρ in Fig. 7b. In contrast to the case in Fig. 7a, now we have the pseudo-thermal buoyancy force acting on the intruder. This additional upward force makes the intruder to rise again beyond $R_\rho > R_{\rho 2}$. Interestingly, the rise-time for $R_\rho > R_{\rho 2}$ decreases with increasing density-ratio, implying that *the heavier the intruder the faster it rises*. Such an effect has been observed in experiments.[12,37,39] Within the window of the RBNP ($R_{\rho 1} < R_\rho > R_{\rho 2}$), we observe that the sink-time varies non-monotonically and diverges at both the limits. For this parameter combination, an intruder with $R_\rho = 1$ will take about 15 cycles of excitation to travel (sink) a distance of its diameter.

With other parameter conditions as in Fig. 7b, we increase the intruder size such that we are in the zone of BNP (see Fig. 1). This is shown in Fig. 8 for three different size-ratios ($R_{ls} = 3, 4, 5$). It is interesting to note that the rise-time is *non-monotoic* with the density-ratio. For a given size-ratio, *there is a threshold density-ratio ($R_\rho < 1$) for the intruder above/below which it rises faster*. This threshold density-ratio shifts to a lower value with increasing size-ratio. Note further that at a given density-ratio *the larger the intruder the faster it rises* in conformity with our earlier observation in Fig. 7b.

Next we fix a large size-ratio of $R_{ls} = 10$, and show the variation of τ with the density ratio R_ρ in Fig. 9 for four different restitution coefficients ($e = 0.999, 0.998, 0.997, 0.99$). With increasing dissipation, the magnitude of the energy-ratio, T_l / T_s, increases that generates additional pseudo-thermal buoyancy force on the intruder, thereby increasing its velocity. Hence the intruder will move

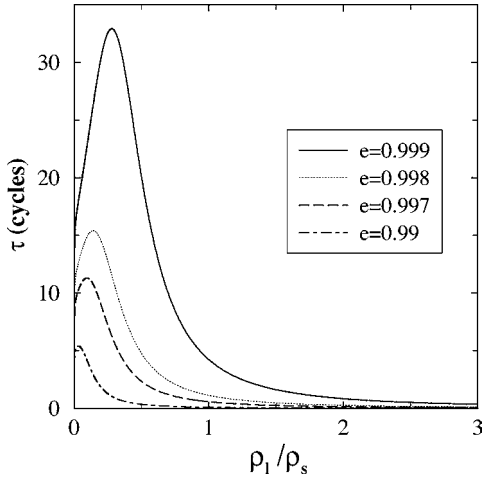

Fig. 9. Variation of rise time τ (in cycles) with density-ratio for different restitution coefficients. The size-ratio is set to $r_l/r_s = 10$; other parameters as in Fig. 8.

faster and the height of the peak in the rise-rate curve decreases as observed in Fig. 9.

5.2. Comparison with Experiments

In order to verify the possible effects of convection,[4] here we make a qualitative comparison of our predictions on the rise time with the recent experiment results of Huerta and Ruiz-Suarez.[39] They performed two-sets of experiments to test the effects of bulk convection, one at $f = 5$ Hz and $\Gamma = 3$ (i.e. the low frequency but high amplitude limit), and the other at $f = 50$ Hz and $\Gamma = 3$ (i.e. the high frequency but low amplitude limit). (They verified that the bulk-convection was negligible in the high frequency limit, but was present in the low frequency limit.) They observed that the rise-time is *non-monotonic* in the high-amplitude (and low frequency) limit (see their Fig. 1), but in the absence of convection the heavier particles sank (see their Fig. 3).

Note that most of the assumptions in our model are in tune with their high frequency experiments since the convection effects are claimed to be negligible in that limit. However, if the level of pseudo-thermal bouyancy force is small, the window of the RBNP ($R_{\rho 1} < R_\rho < R_{\rho 2}$, refer to Fig. 7b) can be made arbitrarily large as in Fig. 7a. In this case, the Archimedean buoyancy force competes with geometric forces, thereby deciding the dynamics of the intruder for $R_\rho > R_{\rho 1}$ as in our Fig. 7a which looks remarkably similar to Fig. 3 in ref. 39.

Moving onto their low frequency experiments, we need to consider the additional effects of bulk-convection. Note that the bulk-convection generates an upward-plume at the center of the container, and two 'narrow' downward plumes near the side-walls; clearly, the granular energy of the particles within the center-plume will be much greater than that of bulk material, and this would lead to another competing force on the intruder. Under the present formalism, this additional force would *reinforce* the pseudo-thermal buoyancy force. Thus, the *effective* pseudo-thermal buoyancy force will increase in the presence of convection, leading to an over-turning of the phase-coexistence line beyond a critical size-ratio (refer to our Fig. 1). Hence the added effect of bulk-convection is to take us to the regime of BNP and the heavier particles will also rise. This is precisely what we see in Fig. 1 of ref. 39. Therefore, in their low frequency experiments, the *effective* pseudo-thermal buoyancy force would compete with the Archimedean buoyancy force and geometric forces.

Lastly, we comment on the experiments of Möbius *et al.*[12] who first showed that the rise-time of an intruder ($r_l/r_s > 10$) in a bed of small particles ($r_s = 250\,\mu$m) is non-monotonic with the density-ratio. They also showed that the peak on the rise-time curve decreases in height and shifts to a lower density with decreasing the air-pressure, and vanishes as the air-pressure approaches 1 torr. It is conceivable that the decreased air-pressure has reduced the *effective* drag on the intruder and thereby increased its velocity—hence the height of the peak (maximum rise-time) decreases with decreasing air-pressure. But the shifting of this peak to a lower density remains unexplained.

6. DISCUSSION

6.1. A Simple Explanation for RBNP: Boltzmann Limit

The reverse segregation effect can be understood by considering the Boltzmann-limit (i.e. the dilute limit $\phi \to 0$) for which the equation of state of species i is

$$p_i = n_i T_i.$$

By integrating the steady vertical momentum equation, we obtain an expression for the number density profile of species i,

$$n_i(z) = n_i(0) \exp\left[-\frac{m_i g z}{T_i}\right], \tag{55}$$

where we have assumed that T_i is independent of z. (This assumption implies that the variation of number-density with z is due to the variation of partial pressure

along z.) Hence, the ratio of number densities is

$$\frac{n_l(z)}{n_s(z)} = \frac{n_l(0)}{n_s(0)} \exp\left[-\frac{m_l}{T_l}\left(1 - \frac{T_l}{T_s}\frac{m_s}{m_l}\right) gz\right]. \tag{56}$$

For a mixture of particles with purely elastic collisions, the equipartition principle holds, i.e., $T_l = T_s$. In this case, the particles segregate according to their masses, driven by the Archimedean buoyancy force, and there is *no* segregation if the particles are of the *same* mass. Thus, the heavier particles remain at the bottom and lighter particles at the top, leading to the RBN effect.

Now considering *inelastic* particles of equal masses $m_l = m_s$ but having different sizes and densities, we know that $T_l < T_s$ for all values of restitution coefficient. This implies that the decay-rate of n_l with z is *faster* than that of n_s. Hence the centre of mass of the larger-particles will be at a lower-level than that of the smaller-particles,

$$\frac{\langle z_l \rangle_{\rm cm}}{\langle z_s \rangle_{\rm cm}} < 1,$$

clearly leading to the RBN effect.

6.2. Higher-order Effects and Possible Experiments

The granular hydrodynamic model is a natural and convenient framework for studying fluidized systems. It is nonetheless criticized for being overly simplified and unrealistic.[14] In our analysis we have considered the hypothesis of a Maxwellian velocity distribution function. Let us remark that the leading–order solution of the Boltzmann–Enskog kinetic equation for granular mixtures is a Maxwellian (see ref. 20), and the non–Gaussian correction term remains relatively small.[31] More importantly, since the present theory is restricted to the Euler-level description of hydrodynamic equations, we do not need to take into account the corrections due to non-Maxwellian effects as explained in ref. 19. Moreover, the Archimedean buoyancy force (F_b^A) and the static geometric force ($F_{\rm ge}^{\rm st}$) do not depend on the distribution function, and the non–Gaussian correction does not affect the dynamic geometric force ($F_{\rm ge}^{\rm dyn}$). Only the pseudo-thermal buoyancy force (F_b^T) can be expressed in terms of the velocity distribution function. Thus, the higher-order corrections would affect this bouyancy force—a detailed investigation of this is left for a future investigation.

All the segregation forces are indirectly measurable in a standard vibrated–bed setup, and thereby making them directly verifiable via experiments. For example, the thermal buoyancy force (F_b^T) can be measured by measuring the granular energies (T_l and T_s) from the snapshots of successive particle configurations. These snapshots can also be used to measure the pair correlation function (χ_{ij} and hence the compressibility factor Z_i) and the dynamic geometric force ($F_{\rm ge}^{\rm dyn}$). The

other two forces (F_b^A and $F_{\rm ge}^{\rm st}$) are then easily obtained. Knowing all these forces from experiments, one could construct each term of our theory independently. We hope that the present investigation will stimulate future experiments to measure these quantities.

7. SUMMARY AND CONCLUSIONS

One of our motivations has been to explore whether the hydrodynamic–description of granular materials can be applied to the derivation of a time–evolution equation for the segregation velocity of intruders in a dense fluidized bed. We have done that in our previous paper,[19] starting from the kinetic-theory of binary mixtures. Based on this time–evolution equation, here we have tried to provide a unified theoretical description for the segregation dynamics of Brazil-nuts in a vibrated granular mixture.

We have discussed a novel mechanism for segregation and argued that the onset of segregation is due to a competition between the *buoyancy* and *geometric* forces. Apart from the standard Archimedean buoyancy force, we have introduced the notion of a pseudo-thermal buoyancy force that results from the fact that the intruder particle fluctuates at a *different* energy level than the smaller particles. (The microscopic dissipation, due to the inelastic nature of particle-collisions, is responsible for the non-equipartition of granular energy.) The size-difference between the intruder and the bed-material results in two geometric forces, one compressive and the other-one tensile in nature– the net geometric force is always compressive. Thus, the net buoyancy force competes with the net compressive geometric force, thereby deciding the onset of BNP/RBNP transition.

For a mixture of perfectly hard-particles with elastic collisions, the pseudo-thermal buoyancy force is zero but the intruder has to overcome the net compressive geometric force to rise. For this case, the competition between the net geometric force and the Archimedean buoyancy force yields a threshold density-ratio, $R_{\rho 1} = \rho_l/\rho_s < 1$, above which the *lighter intruder sinks*, thereby signalling the *onset* of the *reverse buoyancy* effect. For a mixture of dissipative particles, on the other hand, the non-zero pseudo-thermal buoyancy force gives rise to another threshold density-ratio, $R_{\rho 2}$ ($> R_{\rho 1}$), above which the intruder rises again.

This theory is applied to study the dynamics of a single intruder (i.e. in the tracer limit of intruders) in a vibrofluidized granular mixture, with the effect of the base-plate excitation being taken into account through a 'mean-field' assumption. The rise (/sink) time *diverges* near the threshold density-ratio for reverse-segregation. The most interesting result is that the rise-time of the intruder could vary *non-monotonically* with the density-ratio. For a given size-ratio (in the zone of BNP), there is a threshold density-ratio for the intruder at which it takes maximum time to rise and above(/below) which it rises faster. This implies that

the heavier (and larger) the intruder, the faster it ascends; a similar effect has been observed in some recent experiments.[12,39] The peak on the rise-time curve decreases in height and shifts to a lower density-ratio as we increase the magnitude of the pseudo-thermal buoyancy force.

The main message emerging from our analysis is that the pseudo-thermal buoyancy force that results from the non-equipartition of granular energy ($T_l \neq T_s$) plays an important role in the segregation process. Even though the source of this energy non-equipartition is inelastic dissipation, it can be argued that the effects of the bulk-convection will also lead to a separation between the granular energies of the intruder and the bed-particles even in the limit of perfectly elastic collisions. Thus, the increased pseudo-thermal buoyancy force (i.e. with increasing dissipation-levels in our model) can also be related to the presence of the bulk-convective motion. In this connection it may be pointed out that a different functional form for the equation of state (Eq. 6) might change the precise threshold of segregation, but the presence of additional pseudo-thermal buoyancy force, for example, due to convection, is likely to retain the overall phase-diagram similar.

It is remarkable that our theory can explain several experimental observations in a unified manner, despite having many simplifying assumptions. In addition to explaining the experimental results of Breu *et al.*[13] on the reverse Brazil-nut segregation, we have suggested a plausible explanation for the *origin* of the onset of the reverse-buoyancy effect of Shinbrot and Muzzio[10] as well as the *origin* of the non-monotonic ascension-dynamics.[12,39] However, the effects of air-pressure on the non-monotonic ascension-dynamics[12] seems to be more subtle and needs further work. This can be done by considering a three-phase mixture, with separate balance equations for the air and taking into account the resulting interactions on both the smaller particles and the intruders. Lastly, the effects of Coulomb friction and the particle roughness need to be incorporated in our model in future.

ACKNOWLEDGMENTS

The work on ‘reverse segregation’ was started when M.A. was a Humboldt fellow at ICA1, Stuttgart, and L.T. was a doctoral student at PMMH, ESPCI, Paris. The idea on ‘reverse buoyancy’ and ‘non-monotonic ascension dynamics’ was pursued at JNCASR. M.A. acknowledges computational facilities and the financial support from the JNCASR (Grant Number: PC/EMU/MA/35 and DRDO/RN/4124) as well as the hospitality of ICA1 (funded by AvH Fellowship).

REFERENCES

1. H. J. Herrmann, J.–P. Hovi, and S. Luding, *Physics of Dry Granular Media* (Kluwer, Dordrecht, 1998); P. G. de Gennes, Granular matter: a tentative view, *Rev. Mod. Phys.* **71**:S374–S382 (1999); J. M. Ottino and D. V. Khakhar, Mixing and segregation of granular materials, *Annu. Rev. Fluid*

Mech. **32**:55–91 (2000); A. Kudrolli, Size separation in vibrated granular matter, *Rep. Prog. Phys.* **67**:209–247 (2004).
2. L. R. Brown, Fundamental principles of segregation, *J. Inst. Fuel* **13**:15–19 (1939); S. B. Savage and C. K. Lun, Particle size segregation in inclined chute flow of dry cohesionless granular solid, *J. Fluid Mech.*, **189**:311–335 (1988).
3. A. Rosato, K. J. Strandburg, F. Prinz, and R. H. Swendsen, Monte Carlo simulation of particulate matter segregation, *Phys. Rev. Lett.* **58**:1038–1040 (1987).
4. J. B. Knight, H. M. Jaeger, and S. R. Nagel, Vibration-induced size separation in granular media: the convection connection, *Phys. Rev. Lett.* **70**:3728–3731 (1993).
5. J. Duran, J. Rajchenbach, and E. Clément, Arching effect model for particle size segregation, *Phys. Rev. Lett.* **70**:2431–2434 (1993).
6. W. Cooke, S. Warr, J. M. Huntley, and R. C. Ball, Particle size segregation in a two-dimensional bed unergoing vertical vibration, *Phys. Rev. E* **53**:2812–2822 (1996).
7. R. Jullien, P. Meakin, and A. Pavlovitch, Three dimensional model for particle size segregation by shaking, *Phys. Rev. Lett.* **69**:640–643 (1992); S. Dippel and S. Luding, Simulations on size segregation: Geometrical effects in the absence of convection, *J. Phys. I (France)*, **5**:1527–1537 (1995); E. Caglioti, A. Coniglio, H. J. Herrmann, V. Loreto, and M. Nicodemi, Segregation of granular mixtures in the presence of compaction, *Europhys. Lett.* **43**:591–597 (1998).
8. S. Luding, E. Clement, A. Blumen, J. Rachenbach, and J. Duran, The onset of convection in molecular dynamics simulations of grains, *Phys. Rev. E* **50**:R1762–R1764 (1994); T. Pöschel and H. J. Herrmann, Size segregation and convection, *Europhys. Lett.* **29**:123–128 (1995); H. Hayakawa, S. Yue, and D. C. Hong, Hydrodynamic description of granular convection, *Phys. Rev. Lett.* **75**:2328–2331 (1995); J. A. C. Gallas, H. J. Herrmann, T. Pöschel, and S. Sokolowski, Molecular dynamics simulation of size segregation in three dimensions, *J. Stat. Phys.* **82**:443–450 (1996).
9. N. Shishodia and C. R. Wassgren, Particle segregation in vibrofluidized beds due to buoyant forces, *Phys. Rev. Lett.* **87**:084302:1–4 (2001).
10. T. Shinbrot and F. J. Muzzio, Reverse buoyancy in shaken granular beds, *Phys. Rev. Lett.* **81**:4365–4368 (1998).
11. D. C. Hong, P. V. Quinn, and S. Luding, Reverse Brazil nut problem: Competition between percolation and condensation, *Phys. Rev. Lett* **86**:3423–3426 (2001).
12. M. E. Möbius, B. E. Lauderdale, S. R. Nagel, and H. M. Jaeger, Size separation of granular particles, *Nature* **414**:270 (2001); K. Liffman, F. Muniandy, M. Rhodes, D. Gutteridge, and G. Metcalfe, A segregation mechanism in a vertically shaken bed, *Granular Matter* **3**:205–214 (2001); D. Sanders, M. R. Swift, R. M. Bowley, and P. J. King, Are Brazil nuts attractive? *Phys. Rev. Lett.* **93**:208002:1–4 (2004).
13. A. P. Breu, H.-M. Ensner, C. A. Kruelle, and I. Rehberg, Reversing the Brazil nut effect: Competition between percolation and condensation, *Phys. Rev. Lett.* **90**:014302:1–3 (2003).
14. L. P. Kadanoff, Built upon sand: Theoretical ideas inspired by granular flows, *Rev. Mod. Phys.* **71**:435–444 (1999); I. Goldhirsch, Rapid granular flows, *Annu. Rev. Fluid Mech.* **35**:267–293 (2003).
15. F. J. Alexander and J. L. Lebowitz, Driven diffusive systems with a moving obstacle: a variation on the Brazil nut problem, *J. Phys. A: Math. Gen.* **23**:L375–L381 (1990).
16. J. A. Both and D. C. Hong, Variational approach to hard-sphere segregation under gravity, *Phys. Rev. Lett.* **88**:124301:1–4 (2002); M. Nicodemi, A. Fierro, and A. Coniglio, Segregation in hard-sphere mixtures under gravity: An extension of the Edwards approach with two thermodynamical parameters, *Europhys. Lett.* **60**:684–690 (2002).
17. J. T. Jenkins and D. K. Yoon, Segregation in binary mixtures under gravity, *Phys. Rev. Lett.* **88**:194301:1–4 (2002).

18. L. Trujillo and H. J. Herrmann, A note on the upward and downward intruder segregation in granular media, *Granular Matter* **5**:85–89 (2003); Hydrodynamic model for particle size segregation in granular media, *Physica A* **330**:519–539 (2003).
19. L. Trujillo, M. Alam, and H. J. Herrmann, Segregation in a fluidized binary granular mixture: Competition between bouyancy and geometric forces, *Europhys. Lett.* **64**:190–196 (2003).
20. J. T. Jenkins and F. Mancini, Balance laws and constitutive relations for plane flows of a dense, binary mixtures of smooth, nearly elastic, circular disks, *J. Appl. Mech.* **54**:27-34 (1987).
21. J. T. Willits and B. Ö. Arnarson, Kinetic theory of a binary mixture of nearly elastic disks, *Phys. Fluids* **11**:3116–3124 (1999); M. Alam, J. T. Willits, B. Ö. Arnarson, and S. Luding, Kinetic theory of a binary mixture of nearly elastic disks with size and mass disparity, *Phys. Fluids* **14**:4085–4087 (2002).
22. V. Garzó and J. W. Dufty, Homogeneous cooling state for a granular mixture, *Phys. Rev. E* **60**:5706–5713 (1999).
23. W. Losert, L. Bocquet, T. C. Lubensky, and J. P. Gollub, Particle dynamics in sheared granular matter, *Phys. Rev. Lett.* **85**:1428–1431 (2000).
24. M. Alam and S. Luding, How good is the equipartition for the transport properties of a granular mixture? *Granular Matter* **4**:137–140 (2002).
25. M. Alam and S. Luding, Rheology of bidisperse granular mixtures via event-driven simulations, J. Fluid Mech. **476**:69–103 (2003); M. Alam and S. Luding, Energy non-equipartition, rheology and microstructure in sheared bidisperse granular mixtures, *Phys. Fluids* **17**:063303:1–18 (2005).
26. A. Barrat and E. Trizac, Lack of energy equipartition in homogeneous heated granular mixtures, *Granular Matter* **4**:57-63 (2002).
27. K. Feitosa and N. Menon, Breakdown of energy equipartition in a 2D binary vibrated granular gas, *Phys. Rev. Lett.* **88**:198301:1–4 (2002).
28. S. Chapman and T. G. Cowling, *The Mathematical Theory of Non–uniform Gases* (Cambridge University Press, Cambridge, 1970).
29. S. Luding, Global equation of state of two-dimensional hard-sphere systems, *Phys. Rev. E* **63**:042201:1–4 (2001); M. Alam and S. Luding, First normal stress difference and crystallization in a dense sheared granular fluid, *Phys. Fluids* **15**:2298–2312 (2003).
30. G. A. Mansoori, N. F. Carnahan, K. E. Starling, and T. W. Leland Jr., Equilibrium thermodynamic properties of the mixture of hard spheres, *J. Chem. Phys.* **51**:1523–1525 (1971).
31. D. Paolotti, C. Cattuto, U. M. Marconi, and A. Puglisi, Dynamical properties of vibrofluidized granular mixtures, *Granular Matter* **5**:75–83 (2003).
32. M. Bourzutschky and J. Miller, Granular convection in a vibrated fluid, Phys. Rev. Lett. **74**:2216–2219 (1995); J. T. Jenkins and M. W. Richman, Boundary conditions for plane flows of smooth, nearly elastic, circular disks, *J. Fluid Mech.* **171**:53–69 (1986).
33. M. Lopez de Haro and E. D. G. Cohen, The Enskog theory for multicomponent mixtures. III. Transport properties of dense binary mixtures with one tracer component, *J. Chem. Phys.* **80**:408–415 (1984); W. Sung and G. Stell, Transport theory of binary mixture with one trace component of disparate mass, *J. Chem. Phys.* **77**:4636–4649 (1982).
34. R. D. Wildman, J. M. Huntley, and D. J. Parker, Granular temperature profiles in three diemnsional vibrofluidized granular beds, *Phys. Rev. E* **63**:061311:1–10 (2001).
35. O. Zik, J. Stavans, and Y. Rabin, Mobolity of a sphere in vibrated granular media, *Europhys. Lett.* **17**:315–319 (1992).
36. M. R. Maxey and J. J. Riley, Equation of motion for a small rigid sphere in a non-uniform flow, *Phys. Fluids* **26**:883–889 (1983).
37. X. Yan, Q. Shi, M. Hou, K. Lu, and C. K. Chan, Effects of air on the segregation of particles in a shaken granular bed, *Phys. Rev. Lett.* **91**:014302:1–4 (2003); H. K. Pak, E. Doorn, and R. P. Behringer, Effects of ambient gases on granular materials under vertical vibration, *Phys. Rev. Lett.* **74**:4643–4646 (1995).

38. S. Warr, J. M. Huntley, and T. H. Jacques, Fluidization of a two-dimensional granular system: experimental study and scaling behaviour, *Phys. Rev. E* **52**:5583–5595 (1995); S. McNamara and S. Luding, Energy flows in vibrated granular media *Phys. Rev. E* **58**:813–821 (1998); P. Sunthar and V. Kumaran, Temperature scaling in a dense vibrofluidized granular material, *Phys. Rev. E* **60**:1951–1955 (1999); R. Mikkelsen, D. Meer, K. Welle, and D. Lohse, Competitive clustering in bidisperse granular gas. *Phys. Rev. Lett.* **89**:214301:1–4 (2002).
39. D. A. Huerta and J. C. Ruiz-Suarez, Vibration-induced granular segregation: a phenomenon driven by three mechanisms, Phys. Rev. Lett. **92**:114301:1–4 (2004); T. Shinbrot, Granular materials: The Brazil nut effect – in reverse, *Nature* **429**:352 (2004).